Progress In Electromagnetics Research C, Vol. 82, 171–183, 2018

Design and Development of a Unit Element Planar Folded Dipole End-Fired Antenna for Aircraft Collision Avoidance System

Debajit De* and Prasanna K. Sahu

Abstract—Aircraft collision avoidance system is an airborne system which is designed to provide the service as a last defense equipment for avoiding mid-air collisions between aircraft. End-fired antenna is suitable to be used in such airborne systems where low aerodynamic drag is urgently required. An effort to develop such an antenna using dipole elements is presented in this paper. Here a unit element planar folded dipole antenna is presented which radiates in the end-fire direction. Split ring resonators inspired artificial materials are incorporated in the design to improve the directivity performance of the proposed antenna, and those materials are loaded in the same plane of the primary dipole radiator. Here suppression of surface wave in the antenna takes place, which results in gain enhancement and also reduction of side lobes which make radiation pattern better. All these proposed antennas are designed and simulated in CST Microwave Studio (MWS) EM tool which is based on time domain solver. The performance and other antenna characteristics have been explored from the simulation results followed by the antenna fabrication and measurement. Quite good agreement is achieved between the simulated and measured results. Much better performance characteristics make this proposed antenna a good candidate for this application.

1. INTRODUCTION

Over the past decade, planar antennas have found wide application in the wireless communication field because of their attractive features such as small size, low cost, ease of fabrication and potential for high efficiency operation. According to the radiation characteristics, planar antennas are classified into two types. One is broadsided planar antennas, and the other is end-fired planar antennas. A broadsided planar antenna always radiates in perpendicular direction with respect to the plane of the antenna. In this category, some well-known topologies are monopole antenna [1], half-wavelength slotted antenna [2], and patch antenna [3]. An end-fired planar antenna has radiation pattern with the maximum of radiation in the azimuth plane of the antenna. The radiation characteristics of the end-fired antenna depend on the antenna structure, through which the surface wave propagates, and the magnitude of that wave. These types of antennas are Yagi antenna [4], helix antenna with end-fire mode [5] and tapered slot antenna [6].

Planar Yagi-Uda antennas have generated a lot of interest in phased array applications due to its suitability for a wide range of applications such as wireless communication systems, power combiner, phased arrays, active arrays as well as millimeter-wave imaging arrays. A Yagi-Uda antenna and a bow-tie antenna with microstrip baluns were proposed with excellent performance at 8–11 GHz [7, 8], and another quasi-Yagi antenna provided good performance at X-band [9, 10] with a 180° planar balun. A folded dipole antenna can be converted to a Yagi-Uda end-fired antenna with ease, and that is a particular interest for which the planar folded dipole antenna is proposed here.

Received 12 January 2018, Accepted 20 March 2018, Scheduled 1 April 2018
* Corresponding author: Debajit De (de.debajit118@ieee.org).
The authors are with the Department of Electrical Engineering, National Institute of Technology, Rourkela, India.

The planar antennas having end-fire radiation are widely preferable in airborne applications for their characteristics such as simplified structure, easy fabrication, cost effectiveness and low aerodynamic profile. Specially in such areas, there is a restriction on the antenna orientation as it should not obstruct the airflow during flight. Hence, end-fired antenna is suitable for being used in these applications. Also to improve the radiation performance of printed end-fired antennas, artificial materials are widely exploited due to their significant enhancement ability in directivity. Recently, various metamaterial lenses have been designed to improve the directivity of the antennas. The inherent characteristics of material elements determine the gain enhancement ability of the material. A tapered slot antenna provides high gain within the narrow frequency band when the antenna is loaded by a zero-index metamaterial with one component of the effective permittivity approaching zero [11, 12]. Again, gain enhancement in broadband for the tapered slot antenna is possible by employing parallel-line structures within it [13].

This paper focuses on the design of an artificial material based unit element planar folded dipole end-fired antenna for Traffic Alert and Collision Avoidance System (TCAS) of civil aircraft. TCAS is an airborne system which protects its aircraft from mid-air collisions with the other aircraft. TCAS sends interrogation with a consistent rate, ostensibly once every second for surveillance of any surrounding aircraft, and it utilizes a recipient for distinguishing the responses to these transmitting signals which are coming from all the transponders of close-by aircraft as shown in Figure 1. For any dangerous situations, TCAS alerts the aircraft pilot by using alarms and displays in the cockpit panel [14]. In the existing TCAS system, four monopole stub elements are used as TCAS directional antenna, and one blade type element is used as TCAS omnidirectional antenna. These antennas are shown in Figure 2. The TCAS directional antenna is mounted on top of the aircraft, and the TCAS omnidirectional antenna is placed at the bottom side of the aircraft. The transmission and reception frequencies of the TCAS antenna are 1.03 GHz and 1.09 GHz, respectively [15].

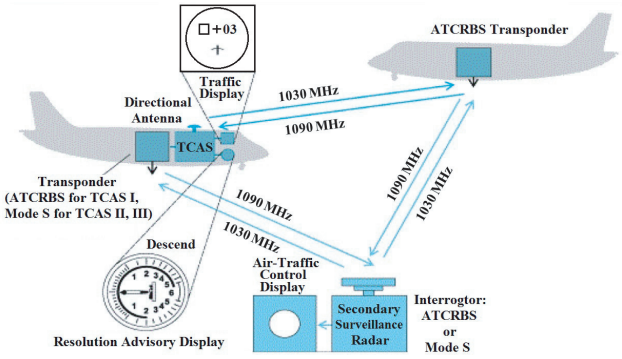

Figure 1. Mid air surveillance.

Figure 2. Existing TCAS antenna.

In this paper, the design methodology of the proposed antenna elements are described in Section 2. Section 3 deals with the simulation and measurement results of those proposed models. The discussions and summary of these results are also included in this section. The conclusion part of this paper is provided in Section 4.

2. ANTENNA CONFIGURATION AND DESIGN ASPECTS

First, a folded dipole planar antenna is proposed here. Thereafter, two more folded dipole planar antennas have been designed and implemented where split ring resonators (SRR) based material are loaded in the same plane of the primary antenna model. The proposed antennas are designed and simulated in CST Microwave Studio (MWS) tool. Here Chemical Etching process is used to fabricate all these antennas. FR4 epoxy is chosen as the substrate material whose dielectric constant (ϵ_r) is 4.4. FR4 Epoxy is a lossy material and is used here since this material is easily available in the market and very much cost effective. 1.06 GHz is chosen as the design frequency since it is center frequency between 1.03 GHz and 1.09 GHz.

2.1. Folded Dipole Antenna without SRR Based Material Loading

Figure 3(a) presets the simulated folded dipole planar antenna without the loading of artificial material and the fabricated model has been shown in Figure 3(b). Figure 3(c) shows the overall layout of the proposed antenna. The antenna has two identical arm radiators which are oriented at 45° direction in the azimuth plane of the antenna. These two arms are printed on the top and bottom sides of the substrate. Both these radiators are fed by coupled balanced parallel strips. 45° angle is chosen for low mutual coupling between adjacent elements as compared to that for 30° and 0° in the case of phased array applications.

In addition to the basic dipole radiator, two folded metallic directors and one truncated slotted ground plane are also designed at the top and bottom of the substrate, respectively. Those two identical parasitic directors are also treated as radiators, and the antenna should have a front-to-back ratio of

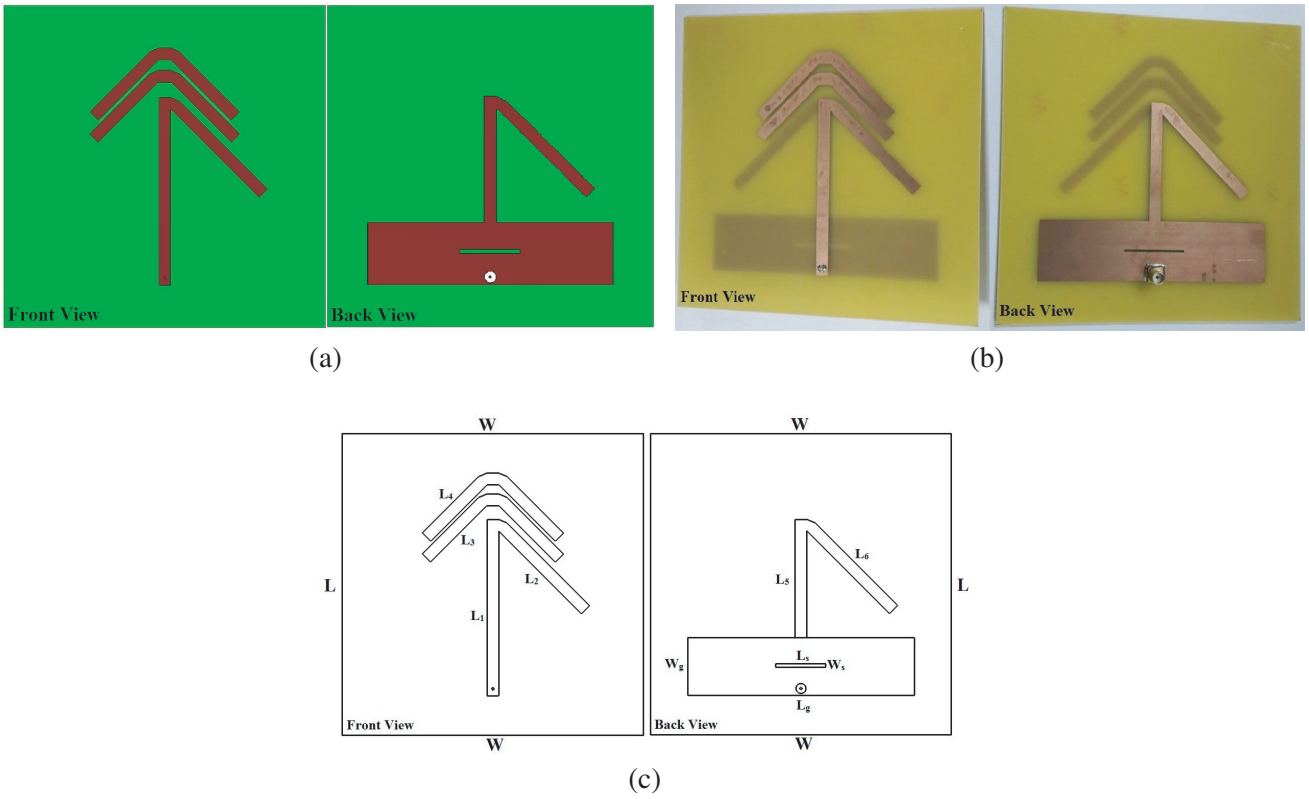

Figure 3. Proposed antenna model without SRR based material loading. (a) Simulated, (b) fabricated, and (c) overall layout.

Table 1. Dimensions of the proposed antenna.

Section	Dimension (In millimeter)
L_1	76.02
L_2 & L_6	63.6
L_3 & L_4	34.5
L_5	51
W_g & L_g	25 & 98
W_s & L_s	2 & 15
W & L	130

9–10 dB due to the presence of the parasitic directors. The directivity of the antenna is also increased due to these two secondary radiators. Here the ground plane acts as a reflector.

Dimensions of the feed lines and the dipole elements on both sides of the substrate are almost identical to each other. Initially, the lengths of the radiating elements are calculated as $L = 2L_2 = L_2 + L_6 = 0.5\lambda_0$. Hence, L is 141.5 mm for 1.06 GHz, and the length of each folded dipole element is 70.75 mm. However, the antenna model is optimized in CST MWS EM tool for getting accurate and best possible result. Thereafter, length of all the resonating dipoles is chosen as 63.60 mm. The detailed dimensions of this proposed antenna are listed in Table 1.

2.2. Folded Dipole Antennas with SRR Based Material Loading

The unit cell split ring resonator is presented in Figure 4(a). When two resonators with two different resonant frequencies f_1 and f_2 are coupled in SRR, the coupling changes both resonances by f_m. The frequency shift depends on the coupling values between the two rings. Here f_1 and f_2 are 1.03 GHz and 1.09 GHz, respectively. The SRR can be designed using

$$f_1 = \frac{c}{2L_1\sqrt{\epsilon_{eff}}} \tag{1}$$

$$f_2 = \frac{c}{2L_2\sqrt{\epsilon_{eff}}} \tag{2}$$

$$L_1 = 4b - x - 4w \tag{3}$$

$$L_2 = 4c - x - 4w \tag{4}$$

where c is the speed of light; L_1 & L_2 are the average loop lengths; ϵ_{eff} is the effective permittivity of the substrate; w is the width of the strips. For simulating the model, boundaries of perfect electric conductor and perfect magnetic conductor are fixed at xz planes and xy planes, respectively.

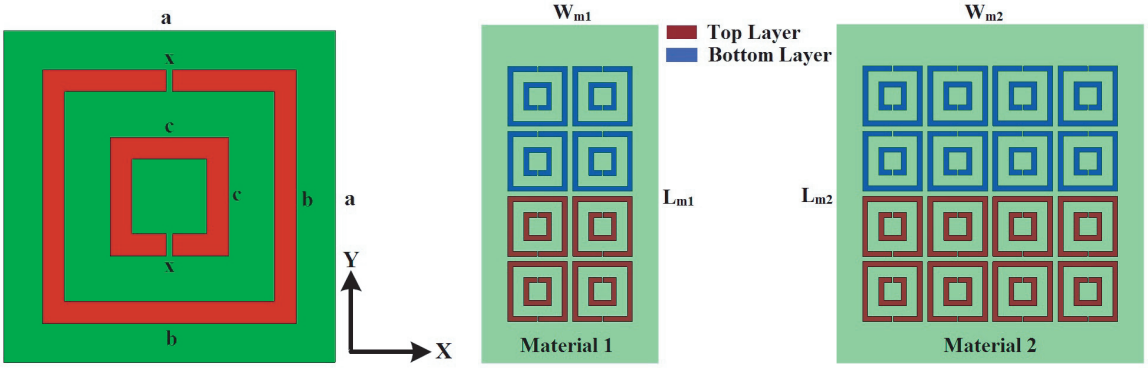

Figure 4. SRR based simulated model. (a) Unit cell and (b) two materials.

Figure 4(b) shows two types of materials which are termed as material 1 and material 2. Material 1 consists of 4 by 2 SRR structures while material 2 has 4 by 4 SRR structures. FR4 epoxy of 1.6 mm thickness is used as the substrate for both the materials. The dimensions of all these models are provided in Table 2.

Now, material 1 and material 2 are loaded in the same plane of the proposed folded dipole antenna. However, the design of the primary antenna section remains identical to before. The simulated and fabricated models of the proposed antenna are shown in Figures 5 and 6. The overall sizes of the proposed folded dipole planar antennas loaded with SRR based material 1 and material 2 are $0.46\lambda_0 \times 0.62\lambda_0$ and $0.46\lambda_0 \times 0.8\lambda_0$, respectively.

Table 2. Dimensions of the SRR unit cell and the proposed antennas.

Section	Dimension (In millimeter)
a	30
b & c	23 & 10.76
x	1
W_{m1} & W_{m2}	68 & 118
L_{m1} & L_{m2}	130

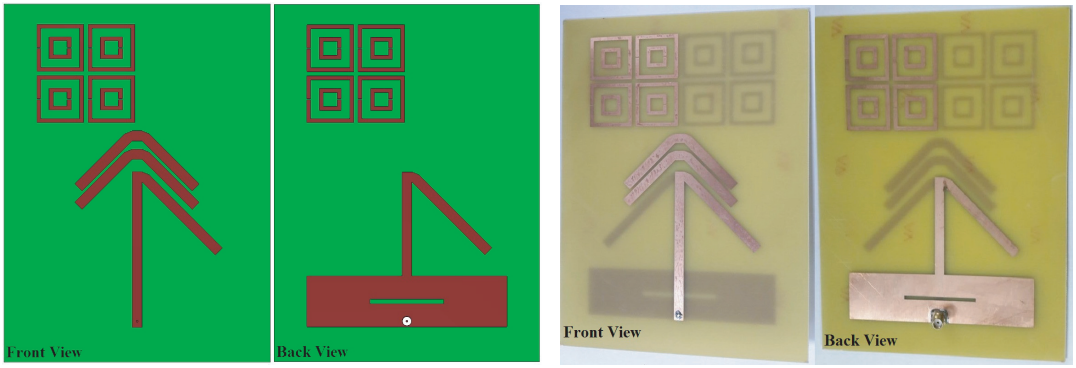

(a) (b)

Figure 5. Proposed antenna model with the loading of material 1. (a) Simulated and (b) fabricated.

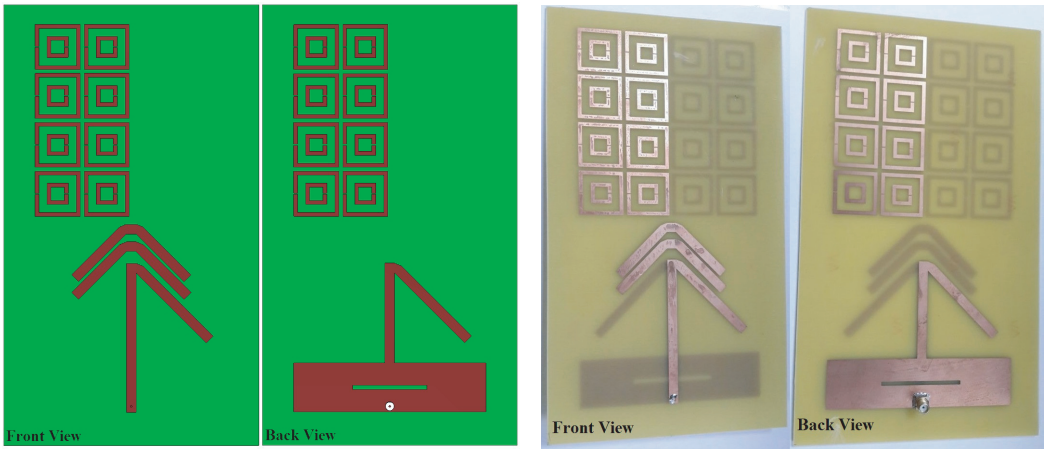

(a) (b)

Figure 6. Proposed antenna model with the loading of material 2. (a) Simulated and (b) fabricated.

3. RESULTS AND DISCUSSIONS

The proposed antennas are simulated, fabricated and tested for the validation of the design technology. Agilent E5071C Vector Network Analyzer (VNA) is used for the measurement and testing purpose. The radiation patterns of these proposed antennas have been measured in a tapered anechoic chamber with 10° step of rotation in the positioner. During the antenna gain measurement, a double-ridge horn antenna is used as the reference antenna.

3.1. Folded Dipole Antenna without SRR Based Material Loading

The simulated and measured return losses of the proposed unit element folded dipole planar antenna are shown in Figure 7. From the simulated return loss plot of the antenna, it is observed that S_{11} is around -33 dB at 1.06 GHz. Again, from the measured return loss plot of the antenna, it is shown that S_{11} is around -22 dB at 1.064 GHz. The measured return loss is in good agreement with the simulated results. However, there are a few disagreements due to measuring environment and fixation of the SMA connectors which are not taken care of during simulation. Figure 8 illustrates the mutual coupling between two folded dipole antennas. Two antennas are separated by a distance of 140 mm which is around $0.5\lambda_0$ at 1.06 GHz. Thereafter, simulation is performed for three times with three different folding angled dipoles. 45°, 30° and 0° are the folding angles of the primary dipole radiators along the XY plane and those angled radiators are printed on the top and bottom sides of the FR4 substrate. Two antennas with similar angled dipoles are used in each simulation. From Figure 8, it can be seen that at 1.06 GHz, the lowest mutual coupling is offered by the antenna which has 45° angled dipole.

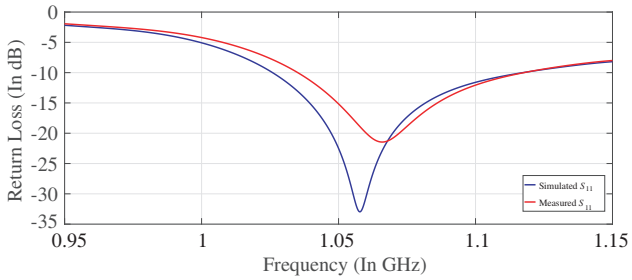

Figure 7. Return loss plot of the proposed antenna.

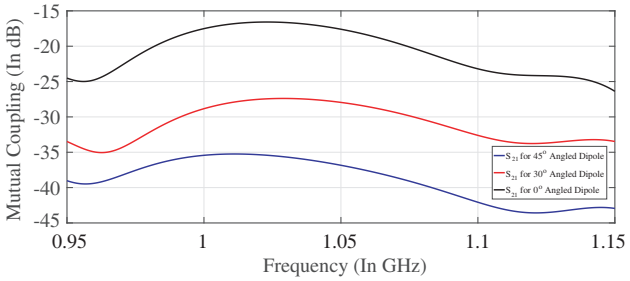

Figure 8. Variation in mutual coupling.

Figures 9(a) and 9(b) show the 3D radiation plots of the proposed antenna for 1.03 GHz and 1.09 GHz, respectively. It is observed that for the two operating frequencies, the simulated 3D radiation patterns are similar.

For 1.03 GHz and 1.09 GHz, the simulated and measured radiation patterns of the proposed antenna are presented in Figure 10(a) and Figure 10(b), respectively. From these figures, it can be seen that the antenna radiates maximum at around $\varphi = 0°$ of the XY azimuth plane for both mentioned frequencies.

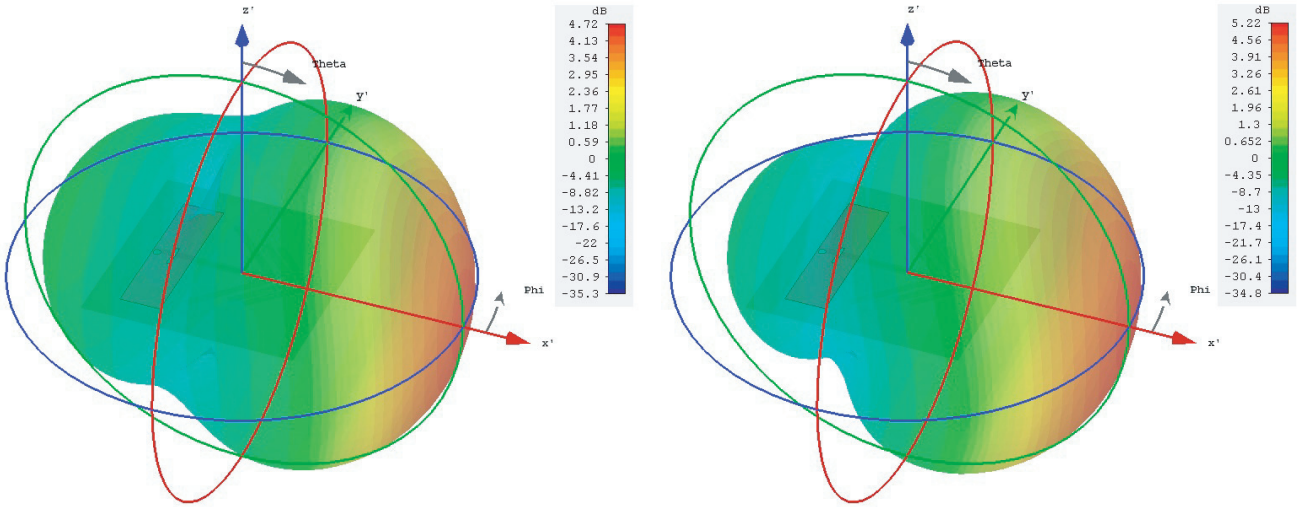

(a) (b)

Figure 9. 3D radiation plots of the proposed antenna for (a) 1.03 GHz and (b) 1.09 GHz.

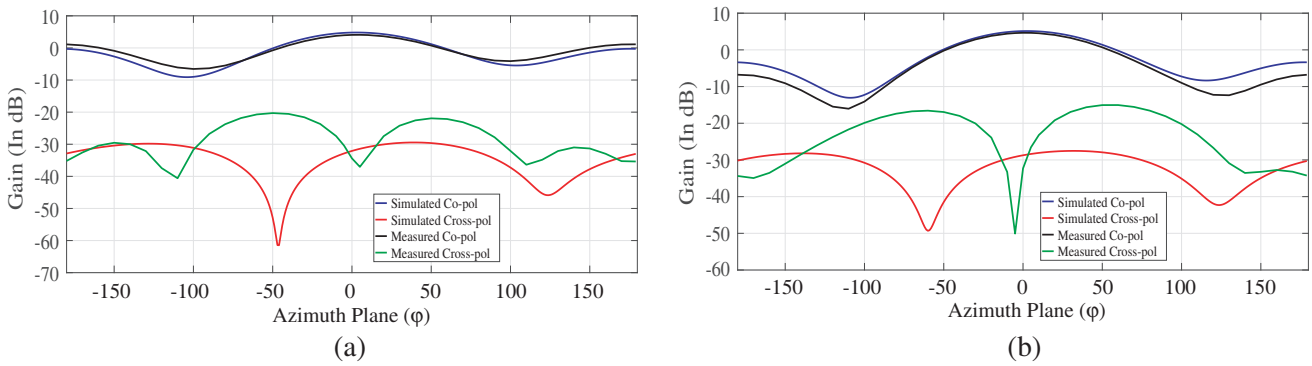

Figure 10. Co and cross polarization of the proposed antenna for (a) 1.03 GHz and (b) 1.09 GHz.

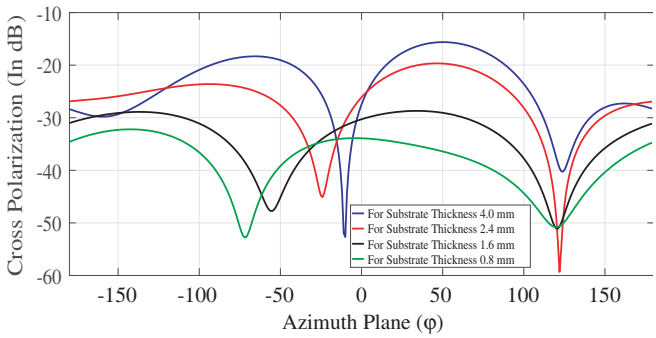

Figure 11. Variation of cross polarization for different substrate thickness.

Table 3. Cross polarization level for various substrate thickness.

Substrate Thickness (In millimeters)	Maximum Cross Polarization Level (In dBW)
0.8	−32.2
1.6	−28.7
2.4	−19.7
4.0	−15.6

Here maximum co-polarization level is around 4.7 dB for 1.03 GHz and 5.2 dB for 1.09 GHz. Furthermore, the maximum cross-polarization level is less than −20 dB. The co-pol is not affected by the cross-pol at both the frequencies.

Figure 11 shows the cross polarization variation for various substrate thicknesses of 0.8 mm, 1.6 mm, 2.4 mm and 4 mm. The dimensions of the proposed antenna are slightly modified in such a way that the antenna can resonate at 1.06 GHz for every case. The maximum cross polarization level for each case is listed in Table 3. From this table, it is observed that the cross polarization level is increased as the substrate thickness is increased. Here the main reason for cross polarization is the vertical electric fields between the dipole arms printed at the top and bottom sides of the substrate.

Figure 12 shows the simulated and measured realized gains of the proposed antenna. It is observed that the simulated antenna gain is around 4.7 dB at 1.03 GHz and around 5.2 dB at 1.09 GHz. The measured antenna gain is around 4.1 dB at 1.03 GHz and around 5 dB at 1.09 GHz. Similarly, the simulated and measured radiation efficiencies of the proposed antenna are presented in Figure 13. Here the simulated radiation efficiency is around 79.5% at 1.03 GHz and around 82.5% at 1.09 GHz, whereas for 1.03 GHz and 1.09 GHz, the measured radiation efficiencies are close to 77% and 81%, respectively.

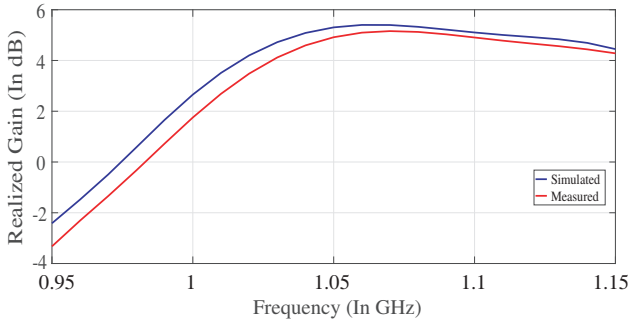

Figure 12. Antenna gain plot.

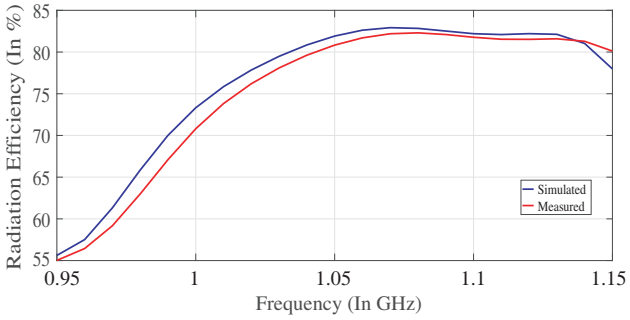

Figure 13. Antenna radiation efficiency plot.

3.2. Folded Dipole Antennas with SRR Based Material Loading

The simulated scattering parameters of the unit cell SRR are shown in Figure 14. Here S_{11} is well below of -15 dB, and S_{21} is close to 0 dB at 1.06 GHz. Hence, the electromagnetic waves can propagate through the material with low return loss. For qualitative analysis, the refractive index (n) of that material is retrieved by using a standard method [16], and the real part of n is shown in Figure 15. For 1.06 GHz, n is around 1.57.

The simulated and measured return losses of the proposed unit element folded dipole planar antennas with SRR based material loading are shown in Figure 16(a) and in 16(b). From the simulated return loss plot of the antenna loaded with artificial material 1, it is observed that S_{11} is around -25.4 dB at 1.06 GHz. Similarly, and from the measured return loss plot, it is shown that S_{11} is around -20.8 dB

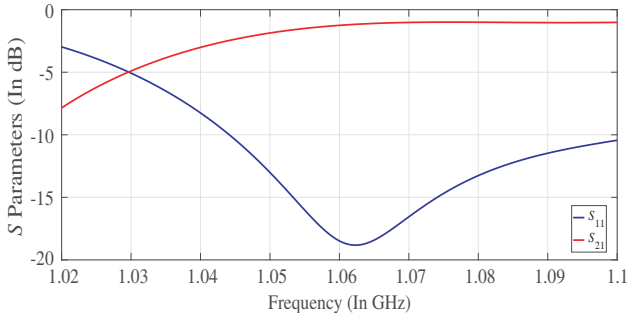

Figure 14. Return loss plot of unit cell SRR.

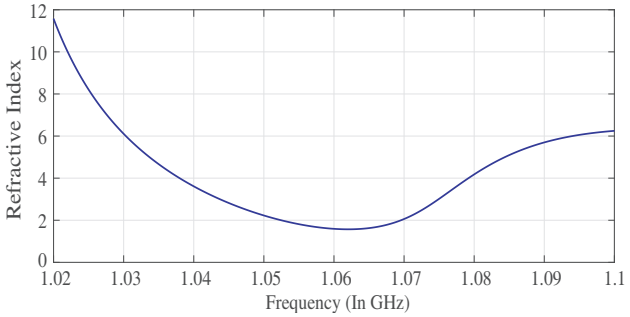

Figure 15. Refractive index plot of unit cell SRR.

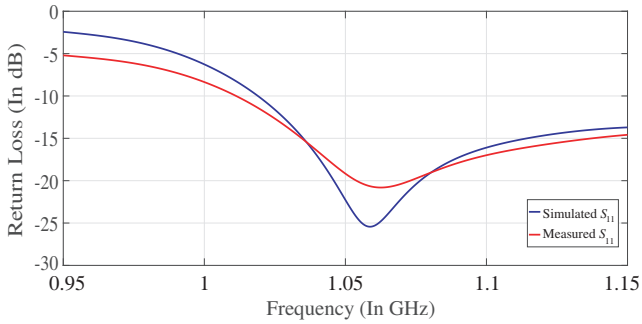

(a)

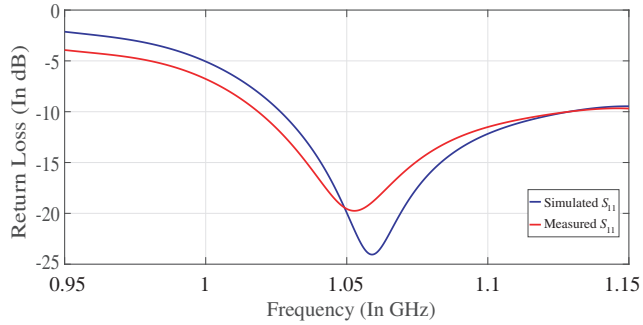

(b)

Figure 16. Simulated and measured return loss plot of the proposed antenna loaded with (a) material 1 and (b) material 2.

at 1.063 GHz. Again, the simulated S_{11} of the proposed antenna loaded with material 2 is close to -24 dB at 1.06 GHz, while the the measured S_{11} is around -19.8 dB at 1.054 GHz.

The Snell's Law states that $n \cdot \sin(\theta) = n_0 \cdot \sin(\theta_0)$, and the electromagnetic wave obeys this law when it propagates through the artificial materials. The EM waves are converged when n is greater than the refractive index of air (n_0). From Figure 15, it is seen that n is greater than 1 at 1.06 GHz. Hence, the phase velocity in the artificial material is lower than that in air. This helps to compensate the phase shift which is produced due to the presence of different materials, and consequently, more phase fronts are obtained. The electric field distributions of the proposed antennas in xy-plane are presented in Figure 17. It is observed that the SRR based material affects the near-field distribution, and the material 2 loaded antenna obtains a larger field intensity than the antenna which is loaded with material 1. Figures 18 and 19 show the 3D radiation plots of the proposed antennas for 1.03 GHz and 1.09 GHz, respectively. It is observed that the simulated 3D radiation patterns are similar for the two operating frequencies.

The simulated and measured radiation patterns of the proposed antennas are illustrated in Figure 20 and Figure 21. For 1.03 GHz and 1.09 GHz, the co and cross polarizations are shown in these figures.

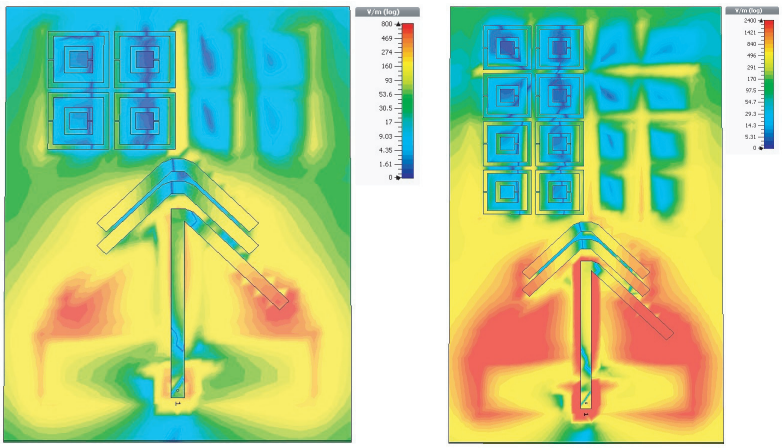

(a) (b)

Figure 17. E-field distribution of the proposed antenna loaded with (a) material 1 and (b) material 2.

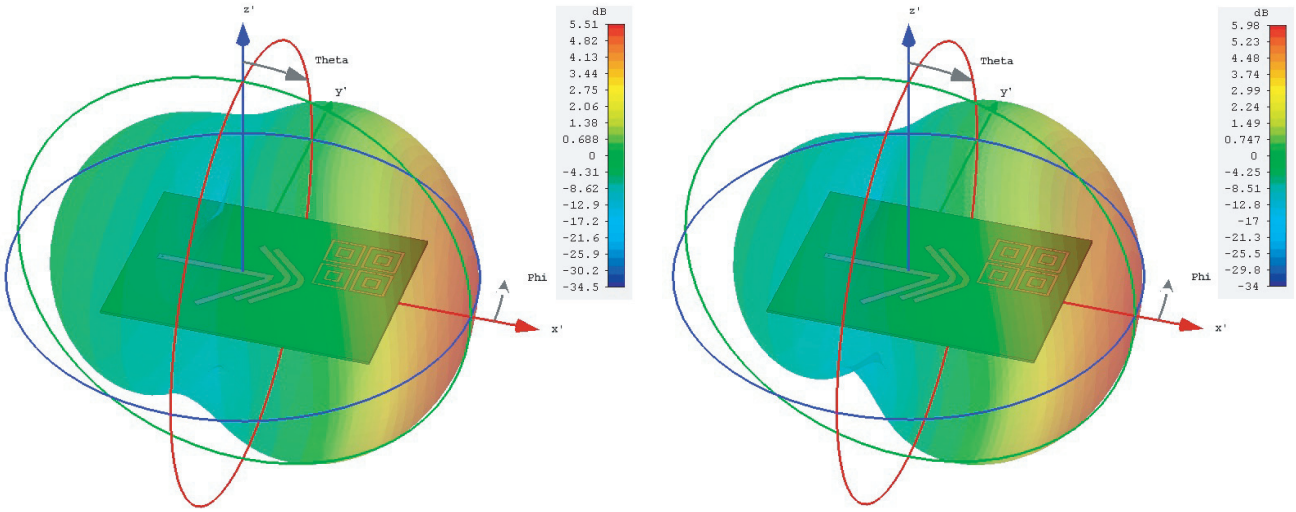

(a) (b)

Figure 18. 3D radiation plots of the antenna loaded with material 1 for (a) 1.03 GHz and (b) 1.09 GHz.

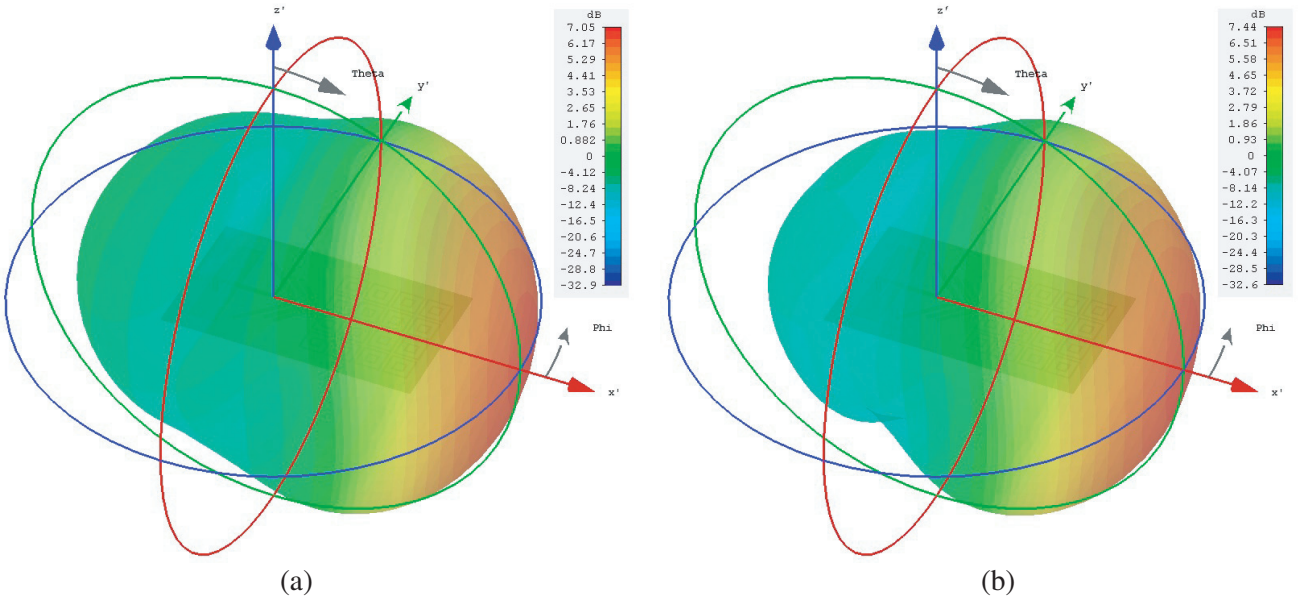

Figure 19. 3D radiation plots of the antenna loaded with material 2 for (a) 1.03 GHz and (b) 1.09 GHz.

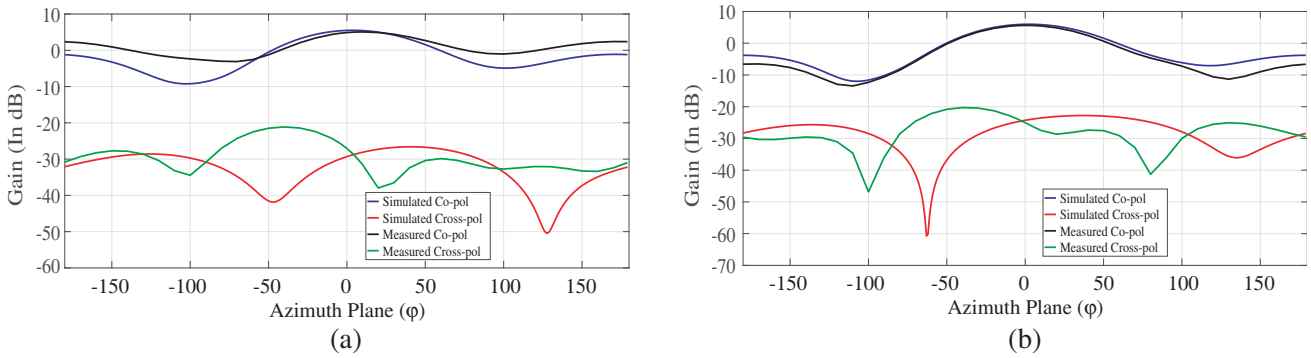

Figure 20. Co and cross polarization of the proposed antenna loaded with material 1 for (a) 1.03 GHz and (b) 1.09 GHz.

It is observed that both the antennas radiate maximum at around $\varphi = 0^\circ$ of the XY azimuth plane for those mentioned frequencies. Here maximum co and cross polarization levels of the antenna loaded with material 1 are close to 6 dB and -21 dB, respectively. Similarly, maximum co and cross polarization levels of the antenna loaded with material 2 are around 7 dB and -20 dB, respectively.

Figure 22 presents the simulated and measured realized gains of the proposed antennas. It is observed that the simulated gain of the proposed antenna loaded with material 1 is around 5.5 dB at 1.03 GHz and around 5.98 dB at 1.09 GHz. The measured gain of that antenna is around 5.17 dB at 1.03 GHz and around 5.7 dB at 1.09 GHz. Furthermore, the antenna loaded with material 2 shows the simulated gains of 7.05 dB at 1.03 GHz and 7.44 dB at 1.09 GHz. For this same proposed antenna model, the measured gains are 6.7 dB and 7.1 dB at 1.03 GHz and at 1.09 GHz, respectively. From this plot, it is clearly understood that the antenna gain is increased as the columns of SRR based structures are increased in the plane of the dipole element.

The simulated and measured radiation efficiencies of the proposed antennas are shown in Figure 23. It is observed that the simulated radiation efficiencies of the proposed antenna loaded with material 1 are around 79.3% at 1.03 GHz and around 81.8% at 1.09 GHz. The measured radiation efficiencies of that antenna are around 72.8% at 1.03 GHz and around 73.9% at 1.09 GHz. Furthermore, the antenna loaded with material 2 shows the simulated radiation efficiencies of 80.2% at 1.03 GHz and 83% at

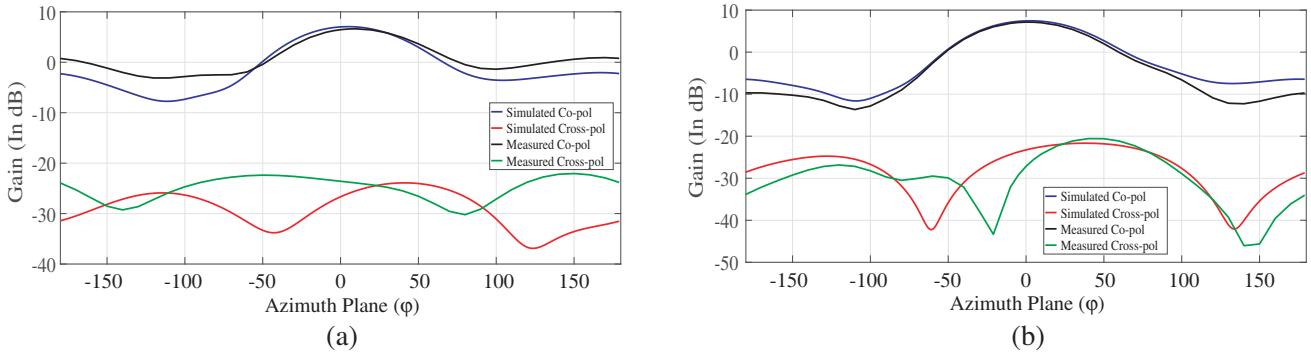

Figure 21. Co and cross polarization of the proposed antenna loaded with material 2 for (a) 1.03 GHz and (b) 1.09 GHz.

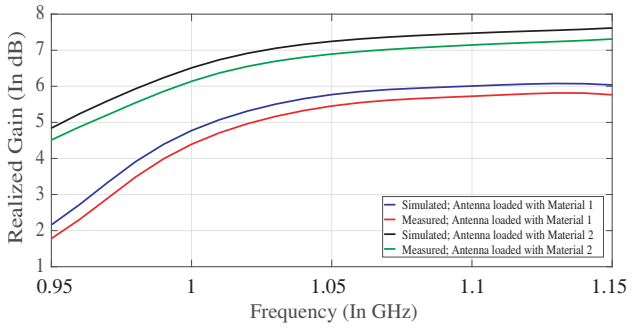

Figure 22. Antenna gain plot.

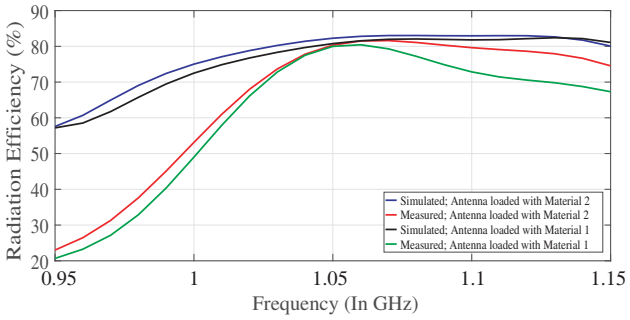

Figure 23. Antenna radiation efficiency plot.

1.09 GHz. At 1.03 GHz and 1.09 GHz, the measured radiation efficiencies of this same proposed antenna are 73.7% and 80.3%, respectively.

3.3. Performance Comparison between the Proposed and the Existing TCAS Antenna

Table 1 summarizes all the simulation and measurement results of the proposed antennas. Here the proposed antennas without the loading of artificial material, loaded with material 1 and material 2 are denoted as antenna 1, 2 and 3, respectively. This table also helps to observe the performance comparison between the proposed and existing monopole TCAS antennas [15]. It is found that the artificial material 2 inspired folded dipole planar antenna provides better performance than the existing monopole TCAS antenna in terms of frequency sensitivity, desired end-fire radiation pattern, gain, beamwidth, and side-lobe level. Hence, this prototype antenna model could be a better product for this application.

Comparing the S parameters as seen from the Table 4, it is clear that the frequency sensitivity is better for the proposed antenna. The VSWR values of the proposed antenna are well matched as that of existing antenna. The gain of the proposed antenna 3 is roughly doubled which implies that the power expenditure during signal transmission is economized. From Table 4, it is also observed that the beamwidth of the proposed antenna is quite reduced as compared to that of the existing TCAS antenna. Due to this narrow beamwidth, resolving the location of the intruder aircraft in terms of bearing angle is much better, and hence the resolution power of this proposed antenna is better than the existing one. As shown in Table 4, the current TCAS antenna which is fitted in the aircraft has the side lobe level of -7 dB, while the side lobe level of the proposed antenna 3 is around -14 dB, and this value is almost half of the said magnitude for the existing antenna. Hence, the sensitivity of the proposed antenna is expected to be better. Due to this low level of side lobe in the proposed antenna and if this low level is considered to be the threshold value of return signal, the covering distance will likely become more than

Table 4. Performance comparison between the proposed and the existing TCAS antenna.

Parameters			Antenna 1	Antenna 2	Antenna 3	Existing TCAS Antenna
fr — Resonating Frequency (In GHz)		Simulated	1.06	1.06	1.06	1.06
		Measured	1.064	1.063	1.054	
Return Loss at fr (In dB)		Simulated	−33	−25.4	−24	−15
		Measured	−22	−20.8	−19.8	
VSWR at fr		Simulated	1.009	1.098	1.097	1 to 1.5
		Measured	1.185	1.295	1.298	
Gain (In dB)	at 1.03 GHz	Simulated	4.7	5.5	7.05	3.5
		Measured	4.1	5.17	6.7	
	at 1.09 GHz	Simulated	5.2	5.98	7.44	
		Measured	5	5.7	7.1	
Beamwidth (In degree)	at 1.03 GHz	Simulated	83.6	76.3	69.2	More than 100
		Measured	83.7	78.5	70	
	at 1.09 GHz	Simulated	83	74.9	70.5	
		Measured	83.1	75.1	71	
Side Lobe (In dB)	at 1.03 GHz	Simulated	−8.2	−8.9	−11.1	−7
		Measured	−7.8	−8	−10	
	at 1.09 GHz	Simulated	−8.5	−9.8	−13.8	
		Measured	−8.1	−9.5	−13.6	
Radiation Efficiency (In %)	at 1.03 GHz	Simulated	79.5	79.3	80.2	-
		Measured	77	72.8	73.7	
	at 1.09 GHz	Simulated	82.5	81.3	83	
		Measured	81	73.9	80.3	

the existing antenna. More aircraft which were hitherto unseen in the existing system can be detected as the covering distance is larger. So, larger number of aircraft can be tracked for collision probability with respect to own aircraft.

4. CONCLUSION

This paper presents a designing technique of artificial material based planar folded dipole antenna which has end-fire radiation, and hence it can be used in many airborne systems such as TCAS and Transponder. The folded dipole antenna loaded with material 2 is very compact in size and weights around 90 grams. Hence this new proposed antenna is also very light in weight as compared to that of existing TCAS antenna whose weight is around 800 grams. This proposed antenna is also cost effective since an FR4 epoxy substrate is used here. The width and length of the substrate are determined for conforming to the space section accessible for the overall fuselage area in the aircraft. The ongoing research focus is on the development of a compact end-fired phased array antenna where this proposed unit element will be used as the array element, and it will be designed in such a way that the whole antenna structure can effectively scan the forward and rear directions with high front-to-back ratio. This proposed antenna will be fitted on the top fuselage of the aircraft, and it will not be left open. It will be encapsulated inside an aerodynamically shaped enclosure, known as radome. For a high speed carrier, a radome of low profile must be used to reduce the air drag. Research on the designing of such shaped encapsulation for this proposed antenna is still going on.

Therefore, the proposed unit element planar folded dipole antenna will be expected to meet the requirements of the advanced avionics standards in terms of design simplicity, lightweight and high performance.

ACKNOWLEDGMENT

The authors would like to acknowledge Thiagarajar Telekom Solutions Limited, Madurai for proving the chance to explore their excellent measurement facilities during this research work. The authors are also very much glad to the college authority of National Institute of Technology, Rourkela, India for various financial support during this research work.

REFERENCES

1. Ammann, M. J. and Z. N. Chen, "Wideband monopole antennas for multi-band wireless systems," *IEEE Antennas and Propagation Magazine*, Vol. 45, No. 2, 146–150, 2003.
2. Booker, H. G., "Slot aerials and their relation to complementary wire aerials (Babinets principle)," *Journal of the Institution of Electrical Engineers. Part IIIA: Radiolocation*, Vol. 93, No. 4, 620–626, 1946.
3. Wong, K. L. and W. H. Hsu, "A broad-band rectangular patch antenna with a pair of wide slits," *IIEEE Transactions on Antennas and Propagation*, Vol. 49, No. 9, 1345–1347, 2001.
4. DeJean, G. R., T. T. Thai, S. Nikolaou, and M. M. Tentzeris, "Design and analysis of microstrip bi-Yagi and quad-Yagi antenna arrays for WLAN applications," *IEEE Antennas and Wireless Propagation Letters*, Vol. 6, 244–248, 2007.
5. Ehrenspeck, H., "The double-helix antenna and its variants, a new class of tunable endfire antennas," *IEEE Transactions on Antennas and Propagation*, Vol. 13, No. 2, 203–208, 1965.
6. Pazin, L. and Y. Leviatan, "A compact 60-GHz tapered slot antenna printed on LCP substrate for WPAN applications," *IEEE Antennas and Wireless Propagation Letters*, Vol. 9, 272–275, 2010.
7. Zheng, G., A. A. Kishk, A. B. Yakovlev, and A. W. Glisson, "Simplified feed for a modified printed Yagi antenna," *IEEE Electronics Letters*, Vol. 40, No. 8, 464–465, 2004.
8. Zheng, G., A. A. Kishk, A. B. Yakovlev, and A. W. Glisson, "A broad band printed bow-tie antenna with a simplified feed," *IEEE Antennas and Propagation Society International Symposium*, Vol. 4, 4024–4027, 2004.
9. Deal, W. R., N. Kaneda, J. Sor, Y. Qian, and T. Itoh, "A new quasi-Yagi antenna for planar active antenna arrays," *IEEE Transactions on Microwave Theory and Techniques*, Vol. 48, No. 6, 910–918, 2000.
10. Leong, K. M. K. H., Y. Qian, and T. Itoh, "Surface wave enhanced broadband planar antenna for wireless applications," *IEEE Microwave and Wireless Components Letters*, Vol. 11, No. 6, 62–64, 2001.
11. Zhou, B. and T. J. Cui, "Directivity enhancement to vivaldi antennas using compactly anisotropic zero-index metamaterials," *IEEE Antennas and Wireless Propagation Letters*, Vol. 10, 326–329, 2011.
12. Sun, M., Z. N. Chen, and X. Qing, "Gain enhancement of 60-GHz antipodal tapered slot antenna using zero-index metamaterial," *IEEE Transactions on Antennas and Propagation*, Vol. 61, No. 4, 1741–1746, 2013.
13. Chen, L., Z. Lei, R. Yang, J. Fan, and X. Shi, "A broadband artificial material for gain enhancement of antipodal tapered slot antenna," *IEEE Transactions on Antennas and Propagation*, Vol. 63, No. 1, 395–400, 2015.
14. Henely, S., *The Avionics Hand Book, 18-TCAS II*, Rockwell Collins, Cedar Rapids, 2001.
15. *TCAS S72-1735-25, AIRNC 735*, Sensor Systems Inc., Aircraft Antennas since 1961.
16. Smith, D., S. Schultz, P. Markos, and C. Soukoulis, "Determination of effective permittivity and permeability of metamaterials from reflection and transmission coefficients," *Physics Review B*, Vol. 65, No. 19, 195104, 2002.